# k-cones and kirigami metamaterials

Keith A. Seffen

*Advanced Structures Group Laboratory, Department of Engineering, University of Cambridge, Cambridge CB2 1PZ, United Kingdom*

(Received 9 May 2016; revised manuscript received 20 July 2016; published 19 September 2016)

We are inspired by the tensile buckling of a thin sheet with a slit to create a foldable planar metamaterial. The buckled shape comprises two pairs of identical e-cones connected to the slit, which we refer to as a k-cone. We approximate this shape as discrete vertices that can be folded out of plane as the slit is pulled apart. We determine their kinematics and we calculate generic shape properties using a simple elastic model of the folded shape. We then show how the folded sheet may be tessellated as a unit cell within a larger sheet, which may be constructed *a priori* by cutting and folding the latter in a regular way, in order to form a planar kirigami structure with a single degree of freedom.

DOI: 10.1103/PhysRevE.94.033003

## I. INTRODUCTION

Figure 1 indicates some of the cone motifs found when certain thin-walled elastic structures are constrained under excessive deformations. A uniform cone is first pulled by its apex through a confining ring to form a second conical indentation, the so-called c-cone [1] [Fig. 1(a)], where c, tautologically, stands for conical. The more familiar d-cone [2] emerges instead when a flat disk, resting on the same ring, is pushed through at its center [Fig. 1(b)]. In this case, we assume that d is for developable, as widely purported. A disk resting on a flat surface is splayed open along a radial cut to produce an e-cone in Fig. 1(c) [3]. Opening as such imposes angular excess around the cone vertex, hence the e prefix; conversely, we may overlap the cut to create angular deficit and another type of d-cone, which is not shown. In forming e-cones or d-cones by manipulating the vertex angle, we are making disclinations i.e., originally axisymmetrical surfaces now with line defects [4]. Finally, a creased disk can be made into a folded conical sheet, or f-cone, in Fig. 1(d), by pushing through and locally inverting the crease. For certain conditions, usually after weakening the crease by repeated flexing, the f-cone can remain inverted by itself [5].

These motifs are found in a range of natural problems, e.g., the coupled twisting and extension of thin strips [6], the packaging and crumpling of paper sheets [7], the out-of-plane shaping of growing biological structures [8], and the textile wrapping and fitting of volumetric shapes by the draper or couturier [9]. When they form, these motifs concentrate Gaussian (double) curvature locally at their vertices while enabling developable deformation elsewhere. Higher deformation this way is energetically more efficient because stretching (or compression) is now relieved in the bulk of the structure outside of the vertices. Of course, vertex plastic strains are inevitable, but they too are highly localized without incapacitating the structure. Controlling motif formation is becoming a rich research topic, particularly for engineering metamaterials with novel responses, as in the f-cone. Here we make a similar proposal based on a cone motif found when a thin, singly slit sheet is put into tension.

Consider the rectangular Mylar sheet in Fig. 2(a). Using a scalpel, a central enclosed slit is made parallel to the short sides. The sheet is pulled normal to the slit by collinear point forces and then anchored by spots of glue. Because the sheet is only 30 $\mu$m thick, it does not remain flat but immediately buckles above the surface. If the experiment is repeated by holding the sheet above the surface and pulling between our fingers, the sheet can displace antisymmetrically about the slit into a different mode shape. Interaction between the sheet and the surface is therefore essential for this mode shape, which comprises four conical regions symmetrically arranged about the slit and separated by flat regions. Each cone is in fact a planar e-cone similar to Fig. 1(c), which is reproduced experimentally in Fig. 2(b) using a Mylar disk. After splaying open the radial cut, around one-third of the disk forms a distinctive conical buckle. This elevated part is not static but can be manually moved around the vertex between the open edges without changing its shape in a neutrally stable manner.

The in-plane stresses leading up to buckling can be compared to those near a slit, or crack, which does not deform out of plane but which can potentially fail by fast fracture under tension. In this case, the stress intensity factor for the crack determines the fracture stress conditions and is denoted by $K$ [10]; in our sheet, because buckling is the limiting response of similarly increasing local stresses, we suggest naming the composite motif as a k-cone, with a lowercase prefix as standard; another reason is presented later. However, before we think about how the stresses might intensify, compressive buckling of a thin plate in tension presents something of a paradox: It is true that tension is applied in the global sense, but the sheet response produces local compression as follows.

The central slit opens horizontally under tension, where the application of point forces ensures that the middle of the slit is more directly pulled apart than its ends, similar to how the open wedge is formed in Fig. 2(b). An e-cone must form at each end of the slit, which causes the flat regions on either side to be pulled inward and to rotate. At the same time, the outline of the open slit becomes trapezoidal and contracts in length, forcing the slit edges to displace upward. This movement couples to the rotations of adjacent horizontal planes, which enables lateral compression in tapering bands away from the slit on both slides, where the points of application of force become a second pair of e-cone vertices. This pair obviously subtends the width of the slit; for the other pair, we find that they consistently have a fixed, or natural, angular width of around 90° for many different proportions of sheet and slit.

Because the composite arrangement is more complex than a solitary e-cone, we expect the natural angular widths of their

 

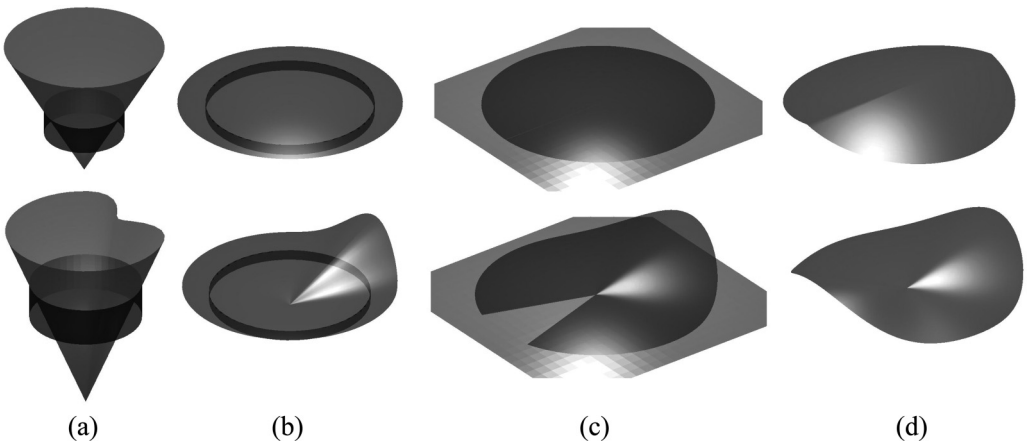


FIG. 1. Various cone motifs described in the literature. In all, the surface is a thin elastic sheet incapable of carrying compressive stresses: The top row is the unstressed initial shape and the bottom row is the deformed cone and its distinctive buckled mode shape where the expediting forces are not shown. (a) A conical cone, or c-cone, formed by pulling a cone vertex through a confining rigid ring. (b) A developable cone, or d-cone, formed by pushing a flat disk supported on a circular rim at its center. (c) A planar e-cone formed by imposing angular excess along a radial cut in a flat disk. (d) A folded cone, or f-cone, formed by locally inverting a folded crease at its center.

respective e-cones to be different. However, researchers over the past 20 years have reported that in certain cone motifs, these widths appear to be invariant irrespective of the size and material of motif, which suggests a common formation mechanism. The width in particular for d-cones and e-cones has been used to express the deformed shape in compact terms, where analytical solutions using large displacement shell equations have been matched against practical measurements. The case of Fig. 2(b), for example, is the planar confined e-cone from [3], whose initial buckled region is predicted to subtend close to 180°. This would seem to be confirmed by Fig. 2(b), but the way in which the detached buckled portion reflects light in the plan view in Fig. 2(b1) suggests a smaller conical width, around 120°–130°. The difference is due to the rate at which detachment occurs, encapsulated by the width of so-called transition regions leading into the cone on either side. These regions are narrow but significant, of the order of 10°–20°, and closer examination of the cone reveals that beyond them the deformed parts are much flatter and connected together by a third transition region over the apex. Thus, the conical deformation has a strong facet character, highlighted schematically in Fig. 2(b3) and recorded in other studies, for example, on d-cones [2].

In this view, elastic deformation is mostly confined to the curved transition regions. If we now imagine their widths becoming infinitesimally thin, the deformed shape is entirely faceted; the e-cone motif can be formed instead by discretely folding along certain lines in a slit disk. Figure 3(a) shows

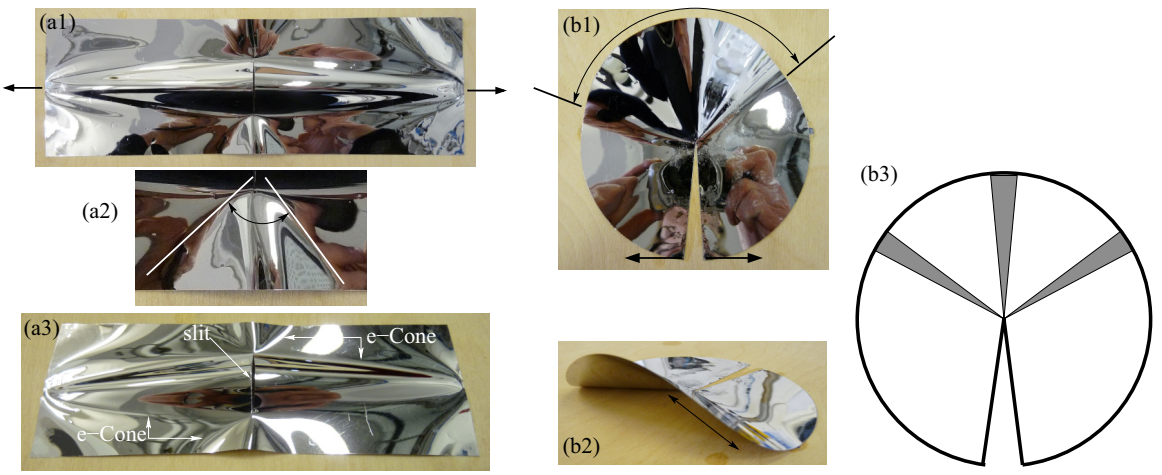


FIG. 2. (a) Slit sheet forming as a k-cone motif under tension: (a1) plan view of a taut Mylar sheet, 18 × 6 cm$^2$ and thickness 30 $\mu$m, with an initial central slit of length 3 cm, pulled apart by collinear forces applied to its sides. The underlying surface constrains the buckled sheet to displace upward and out of plane and to form as four e-cones. (a2) Close-up view of the lower e-cone, highlighting its detached range of around 90°. (a3) Slightly inclined view of (a1) highlighting the out-of-plane shape of the lower e-cone. (b) Planar-confined e-cone. (b1) Plan view after opening a Mylar disk of radius 4 cm. The out-of-plane buckle is highlighted and subtends approximately 125° in the plan. (b2) Different view of (b1) showing the displaced shape. Note the radial opening in the background and the flatness of the nearest detached portions indicated by the double arrow. (b3) Schematic view of (b1) showing the surface either as white flat facets (horizontal or displaced) or as gray regions of adjacent conical curvature.

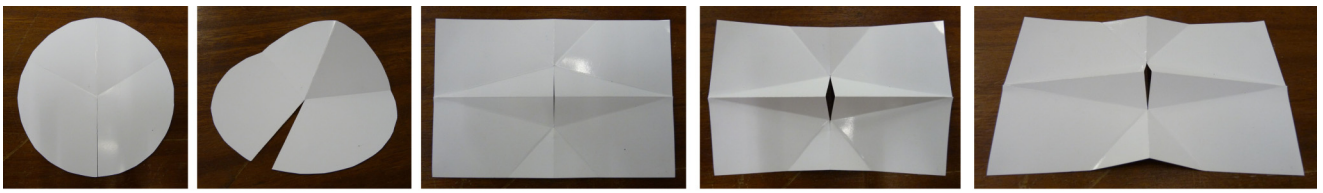


FIG. 3. (a) Discretely folded e-cone made by cutting a paper card disk radially to form a slit before folding along three radial lines: (a1) Plan view before opening and (a2) isometric view to highlight displacements after opening. (b) Discretely folded version of the k-cone motif in Fig. 2(a) made up of four discrete e-cone vertices: (b1) Plan view of initial layout of folds and central slit; (b2) plan view after opening by pulling across the slit, which forms as a trapezoid; and (b3) inclined view of (b2) to observe folding out of plane. In all panels, each vertex has two valley folds and one mountain fold; the flat intervening facets remain flat but rotate in plane as the e-cones fold out of plane.

a symmetrical version made out of paper card. Being much thicker than Mylar, fold lines can be made by scoring without penetrating the card and the intervening facets are much stiffer, so the folded sheet has flat facets and holds its shape. The e-cone is simulated by three fold lines emanating from a common vertex: two valley folds along where the e-cone begins to lift off on either side and one mountain fold along its central ridge. Here the initial separation of the valley folds in the plan is deliberately chosen to be 120° in line with Fig. 2(b).

A discrete k-cone motif can be similarly constructed [see Fig. 3(b)]. The outlines of four e-cone vertices are scored onto a flat rectangular card with an enclosed slit before folding out of plane. The angular width of the vertex pair at the slit ends is initially set to be 90° to match the natural continuum width. As usual, the other pair subtends the slit width from points in the middle of parallel edges. Overall, the folded card resembles an origami structure, but it is not because we have had to cut the card to make the slit, which is strictly forbidden [11]; it is a kirigami structure (from Japanese *kiru*: to cut) and the previous soubriquet, k-cone, is also fitting. When the card is pulled apart by increasing forces, the rate of folding quickly diminishes; we observe the same tempering of deformation in the continuum case. If instead we pinch e-cones between our fingers for even higher deformation, the narrower e-cones may be closed into a single vertical plane with a mountain rotation equal to 180°; correspondingly, the wider pair is partially folded to some angle set by the geometry of sheet. If the narrower e-cones happen to subtend the slit, the slit ends eventually meet each other. All of these features are demonstrated later and usefully exploited.

The above brings us, rather circuitously, to the aims of this paper. We wish to focus on discretely folded structures because their operation is simpler and their analysis is largely algebraic in nature. We are also able to draw upon an important property of discrete vertices in determining how they may be folded: that the angular deficit imposed at a given vertex is equal to the area of the Gauss mapping of facet normal vectors. The method was originally applied to d-cones in [12] and recently extended for e-cones in [13]. We repeat the derivation for clarity's sake and we solve for the fold angles between symmetrically arranged facets. We then endow fold lines as linear torsional springs, as if to concentrate the elastic deformation of the continuum case into its narrow transition regions [cf. Fig. 2(b3)]. We compute the strain energy stored and the external work performed on the system before seeking minimal energy and hence equilibrium configurations. We are then able to predict the width of our solitary e-cones as well as the near right-angled e-cones in the continuum k-cone motifs. We can then infer some facts about the relative folding properties of a given layout of discrete k-cone. Although this is restricted to the small displacement regime throughout, we can surmise the shape of more heavily folded k-cones (by themselves and when they are interconnected, in order to synthesise an extensive sheet), our foldable metamaterial. We then conclude.

## II. DISCRETE e-CONES AND k-CONES

Figure 4(a) indicates the planar geometry of a discretely folded e-cone with four facets A–D. The valley folds are symmetrically separated by angle $2\beta$ with respect to the mountain fold, which is parallel to the radial slit. Other nonsymmetrical configurations are possible but are not of immediate interest. Facets A and B are separated by opening the slit into a planar wedge subtending angle $2\alpha$, which is the angular excess imposed at the vertex: The other facets C and D rotate out of plane as the mountain fold tilts upward. When $\alpha$ is zero, there are no fold rotations, and displacements are small enough everywhere so that the original planar layout of fold lines does not change in the deformed plan view. We also assume that the sheet thickness is negligible compared to the disk radius $r$, so it does not interfere with the folded geometry even for large rotations.

The mountain fold rotation is denoted by $\phi$ and for the valleys as $\theta$. Moving around the vertex counterclockwise gives us the vector direction of rotation according to the right-hand screw rule: For a mountain fold rotation, its vector must point toward the vertex while a valley one points away. Each vector is now plotted in Fig. 4(b) moving from facets B to C, C to D, etc., which reveals a closed vector triangle where $2\theta \cos\beta = \phi$. However, as carefully described in [12], this vector triangle is identical to the Gauss mapping of vectors normal to each displaced facet onto the so-called unit sphere [14]. Furthermore, the area enclosed by this spherical mapping is precisely the angular deficit $2\alpha$ imposed at the vertex. Given the small nature of rotations, this mapping, viz., Fig. 4(b), is a planar figure of simple area $(\phi/2)\theta \sin\beta$. Note that the circulation of vectors is clockwise, in the opposite sense to the construction sequence, suggesting that our area is strictly negative; however, recall that angular deficit is defined to be positive, so there is no conflict of sign when there is actually angular excess. After some manipulation, we find the

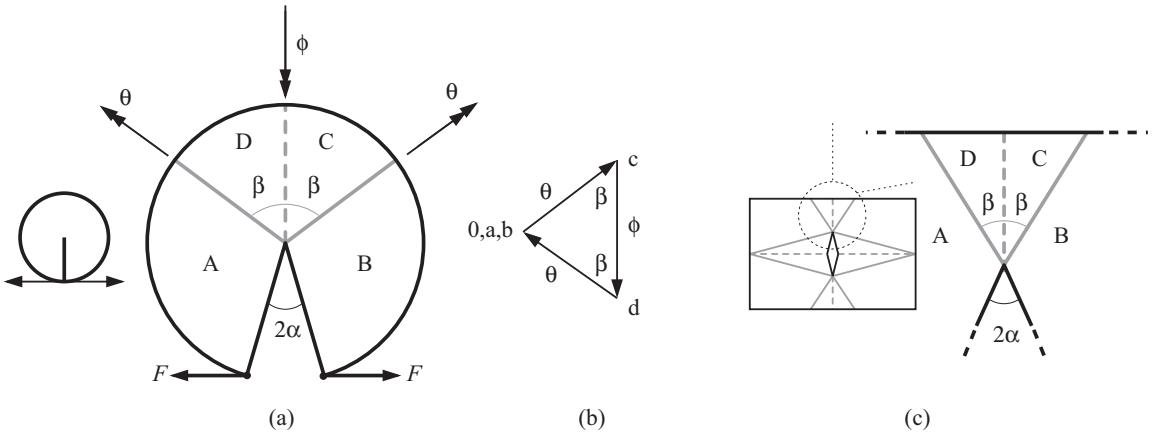


FIG. 4. Schematic plan layout of a discretely folded e-cone. (a) The disk is pried apart along a radial slit by a pair of forces $F$ to give an angular separation of $2\alpha$. Valley folds are drawn as solid gray lines separated by $\beta$ on either side of the single mountain fold shown as a dashed line; their respective rotations are $\theta$ and $\phi$. (b) Gauss mapping for the rotation vectors from (a). These are drawn when circulating counterclockwise around the central vertex; lowercase letters denote the particular facets in uppercase from (a), and a 0 signifies a datum rotation of zero. (c) Rendering of an e-cone at the top of the slit in a k-cone motif as a discrete e-cone whose valleys and mountain folds have unequal lengths compared to (a). The angular excess imposed at the vertex is also $2\alpha$, and in all cases $\alpha$ has been shown somewhat exaggerated in size.

compatibility relationships for a discrete e-cone as

$$\phi = \sqrt{\frac{8\alpha}{\tan\beta}}, \quad \theta = \sqrt{\frac{4\alpha}{\sin 2\beta}}. \tag{1}$$

Each fold line behaves like a torsional spring elastically resisting out-of-plane rotation between pairs of facets. This simulates the concentrated deformation in the real transition regions, so each spring stiffness is akin to the well-known flexural rigidity of elastic plates [14]; fortuitously, there is evidence to suggest that actual fold lines behave this way [15]. Our purpose is to find a natural value of $\beta$ if our discrete e-cone represents a first-order approximation of the continuum case.

Let $k$ be a constant rotational stiffness of fold per unit length of line with units N m/rad m. The strain energy stored in a fold must be $(k/2) \times (\text{rotation})^2 \times (\text{length})$, which amounts to $2(k/2)r\theta^2 + (k/2)r\phi^2$ for the folded e-cone. The wedge angle is opened by a pair of equal and opposite forces $F$, as shown in Fig. 3(a). These remain collinear and planar while performing positive work equal to $2F\delta$, where $\delta$ is the displacement of the line of action of each force $r\sin\alpha$. This work is then subtracted from the stored energy to reveal the total conservative potential of the system $U$ as

$$U = 4kr\alpha\left[\frac{1}{\sin 2\beta} + \frac{1}{\tan\beta}\right] - 2Fr\sin\alpha \tag{2}$$

when $\phi$ and $\theta$ are substituted from Eq. (1).

Assuming that $k$ and $r$ have specified values, $U$ is a function of three parameters $\alpha$, $\beta$, and $F$, although $\alpha$ is the only generalized coordinate, our single degree of freedom. There are no dissipative or inertia terms and thus equilibrium configurations are given by differentiating $U$ with respect to $\alpha$ and setting equal to zero to yield

$$F = \frac{2k}{\cos\alpha}\left[\frac{1}{\sin 2\beta} + \frac{1}{\tan\beta}\right]. \tag{3}$$

When the slit is closed, $\alpha = 0$ and $\cos\alpha = 1$, giving nonzero $F$. Alternatively, if $F$ is increased from zero, there is no deformation until each force reaches a threshold value defined by $\cos\alpha = 1$ in the above expression: This is the buckling load for a folded e-cone. Afterwards, $F$ rises nonlinearly with increasing gradient with respect to $\alpha$ as it approaches the asymptote at $\alpha = 90°$. Such variation generally reflects what we see beyond small displacements, that ever higher forces are needed to open the e-cone further. The specific variation in $F$ also depends on $k$, but we are not interested in finding this; instead, we seek the natural value of $\beta$, which is found from stationary values of $U$ with respect to $\beta$. This calculation is trivial and does not depend on $k$, resulting in a final characteristic equation $\cos^2\beta + (1/2)\cos 2\beta = 0$ with an exact solution of $\beta = 60°$ (in the range 0° to 90°). This give us a total angular width of 120°, which is a fair result given the crudeness of Fig. 2(b), and a buckling load $F/k = 2\sqrt{3}$.

The same model can be applied to the k-cone motif. Our potential function only needs to consider the unconstrained e-cone pair; the contribution from the other pair subtending the slit is only required if we wish to compute the applied forces. Assuming a symmetrical layout in Fig. 4(c), the corresponding valley folds are longer than the mountain fold by a factor of $1/\cos\beta$, which also multiplies the $1/\sin 2\beta$ term in the strain energy component of Eq. (2). Minimizing this component with respect to $\beta$ sets $1 - (3/2)\cos^2\beta - \cos^3\beta = 0$, which gives a solution of $2\beta = 94.6°$ [cf. around 90° in the continuum case in Fig. 2(a)].

We are not interested in the variation of the applied forces any further but now focus on the kinematics of a discrete k-cone for developing our metamaterial. The description is a straightforward extension of the result for a single e-cone [Eq. (1)], when we consider how the deformation couples between adjacent pairs of e-cones. Figure 5(a) indicates the initial planar geometry of the sheet, slit, and fold lines. We label the two vertices at the slit ends as $A$ and $A'$, which have the same fold line pattern: When the sheet is flat, the symmetrical

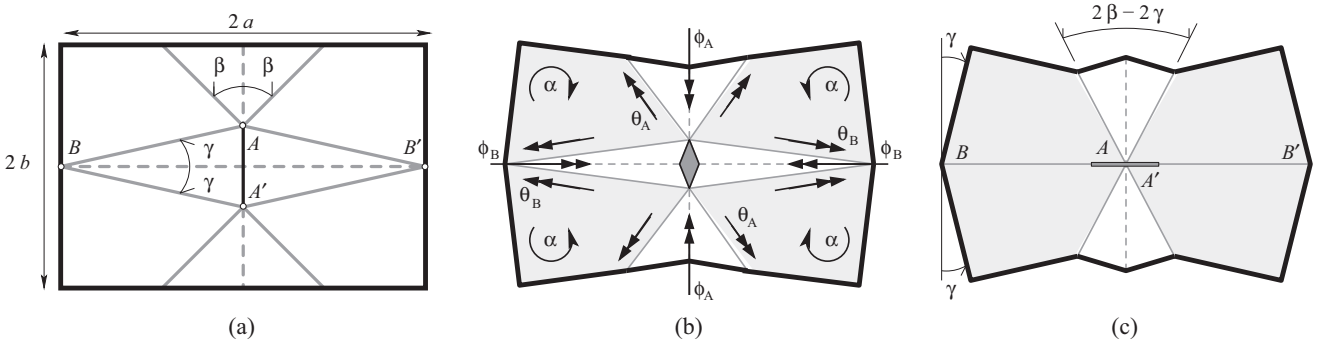


FIG. 5. Schematic layouts of the discretely folded k-cone motif from Fig. 3. (a) Initial unfolded sheet. The side lengths are $2a$ and $2b$ and the four vertices are circles labeled $A$ and $A'$ at the top and bottom ends of the slit and $B$ and $B'$ in the middle of the sides. The e-cones are described by valley folds drawn as solid gray lines and mountain folds as dashed lines; the central slit has a black boundary. Angles $\beta$ and $\gamma$ describe the width of e-cones and the length of slit. (b) Partially folded shape in which each flat facet, shaded light gray, rotates by $\alpha$. The corresponding valley fold rotations are $\theta$ and mountain fold rotations are $\phi$. (c) Fully folded shape for this geometry, where $\beta > \gamma$. The vertices at $B$ and $B'$ are folded vertically and close while $A$ and $A'$ remain open. The slit configuration has rotated, which can be confirmed in Fig. 6.

width between the valley folds is measured by the usual $2\beta$, which retains a general value since we can specify the fold line layout. For the other vertices $B$ and $B'$, the equivalent angular width is set by $2\gamma$, which also sets the slit length to be $2a\tan\gamma$ for a transverse side length of $2a$; conversely, the slit length determines $\gamma$. The sheet width is $2b$, which with $2a$ is assumed to be much larger than the sheet thickness as usual.

The folded shape in Fig. 5(b) shows first the flat regions between e-cones rotating in-plane by the same angle in the required sense. We set this angle to be $\alpha$, giving the usual angular excess of $2\alpha$ for each vertex. As the facets rotate upward, all valley folds for the $A$ and $A'$ e-cones undergo the same rotation $\theta_A$ and their mountain folds rotate by $\phi_A$; for the $B$ and $B'$ e-cones, the equivalent fold lines rotate by $\phi_B$ and $\theta_B$, respectively. Transcribing expressions from Eq. (1) directly with appropriate subscripts, we have

$$\phi_A = \sqrt{\frac{8\alpha}{\tan\beta}}, \quad \theta_A = \sqrt{\frac{4\alpha}{\sin 2\beta}};$$
$$\phi_B = \sqrt{\frac{8\alpha}{\tan\gamma}}, \quad \theta_B = \sqrt{\frac{4\alpha}{\sin 2\gamma}}. \qquad (4)$$

Recall that these expressions are only valid for small fold rotations. They do confirm, for example, that the narrower e-cone pair folds more quickly and hence is likely to close first. In fact, the shape of the other wider e-cone pair is straightforward to calculate in this final state, assuming that $\beta > \gamma$, say: The flat parts have rotated by $\alpha = \gamma$ and the wider e-cones now subtend $2(\beta - \gamma)$ in a plan view [see Fig. 5(c)]. Clearly, if $\beta = \gamma = 45°$, the e-cone at $A$ shares its valley folds with $B$ and $B'$ and similarly for the e-cone at $A'$, which can be clearly seen in another demonstrator in Fig. 6(a). Because the e-cones subtend the same angle, their initial rotations are synchronized in Eq. (4) and subsequently for larger rotations, leading to zero width when they fold vertically [see Figs. 6(b) and 6(c)]. In the plan view, the slit opens broadly before closing and reorienting itself by 90°. We then choose to fold the e-cones over in Fig. 6(d) so that the sheet has a minimal out-of-plane thickness.

## III. FOLDED k-CONE SHEET

The discrete k-cone motif behaves as a structural mechanism with a mobility of unity, i.e., it has one degree of freedom where folding couples localized out-of-plane bending to in-plane tension and compression. For planar metamaterials with similarly novel kinematics, e.g., as found in [16], we must focus on creating a structured material, which uses the k-cone motif in a repetitive manner. One way to achieve this is to

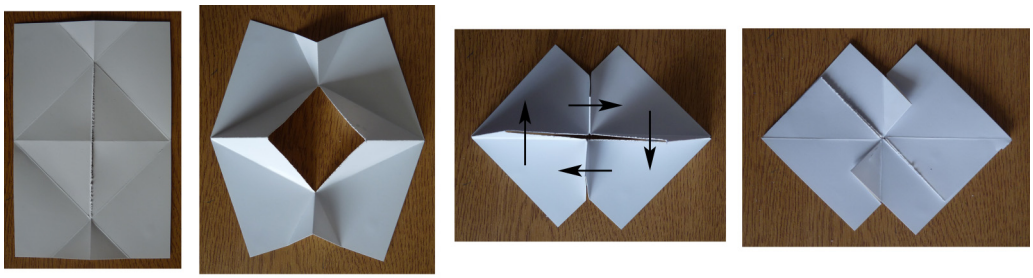


FIG. 6. Fold line layout with $\beta = \gamma = 45°$ so that all e-cones can fully fold and close. (a) Initial geometry. (b) Intermediate configuration with $\alpha \approx 20°$. (c) Fully folded state, $\alpha = 45°$, with all e-cones fully closed and standing upright normal to the page. Note how the slit becomes reconfigured compared to (a). The arrows indicate a second folding stage in which the upright e-cones are folded flat, to give the fully flattened configuration in (d).

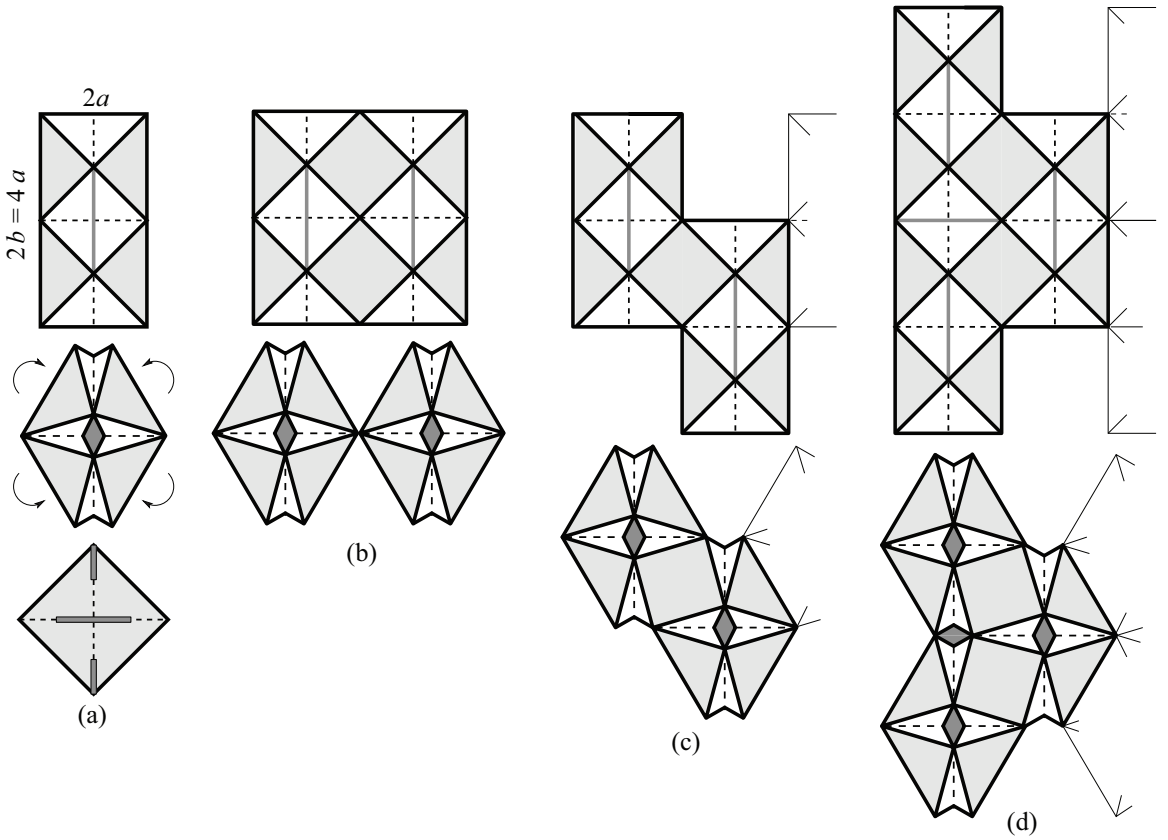


FIG. 7. Tessellation of individual sheets as unit cells within a larger sheet. The unit cell is similar to Fig. 6 but with $b = 2a$ so that the valley folds run to the sheet corners. (a) Shown on top is the plan view of the initial unit cell, the middle shows the partially folded state, and the bottom is the fully folded version with upright closed e-cones, as per Fig. 5(c). Note that the boundary is now square and that the flat facets between e-cones, shaded light gray, have rotated by 45°. (b) Prospective tessellation using (a) twice and side by side. The top shows that the adjacent triangular facets are now connected to form single squares (light gray). The bottom shows the original triangular facets, however, rotated in opposite directions and separated. (c) Alternative side-by-side pairing with a linear offset of $b$ along one side. The top shows adjacent triangular facets again, making a common square. The bottom shows that the rotation of the square is compatible with the original triangular facets and folding can proceed. (d) Formation of a second row by adding a third unit cell to (c). The top shows that adjacent e-cones between rows cannot be connected but are separated by a second, horizontal slit. The bottom shows the partially folded triumvirate, which can be repeated indefinitely. For all subfigures inside each initial unit cell, valley folds are solid black lines at ±45°, mountain folds are dashed at 0° or 90°, and slits are solid gray lines.

lay out the motif as contiguous unit cells in two directions. The boundary outline of the initial motif and that of its folded state must each form as compatible unit cells everywhere and the continuity of fold lines between cells is also important. We must also think about the limits of e-cone folding, which can include the extreme case where all e-cones may be fully folded. By definition, the layout of slits will be a uniform pattern and the final repetitive structure is ideally constructed by first cutting a series of slits and then folding the entire sheet around them in sequence, typically performed from the outset in other studies. We confine attention to planar deformation in the global sense, but others have tackled out-of-plane shaping directly by recognizing that kirigami structures can possess a net amount of Gaussian curvature not available from origami counterparts; this is an inevitable consequence of Gauss's *Theorema Egregium* [14] and successful developments have led to so-called pluripotent materials [17]. Our planar solution is given in Fig. 7.

The unit cell has a very similar layout to Fig. 6 with fold lines at either 0°, 45°, or 90° except that the e-cones at the slit ends subtend the full width $2a$, which sets $b = 2a$ [see Fig. 7(a)]. This yields a fully folded state with a square boundary (unlike, say, Fig. 6) with facets between e-cones being right-angled isosceles triangles rotated by 45° in plane. This folded, or closed, state can potentially tessellate because of its square outline, but if a pair of cells is connected side by side, adjacent triangular facets, which could be connected to form interior squares [see Fig. 7(b)], must cleave apart as they rotate in opposite senses; consequently, this double unit cell is not mobile at all. In order to match rotations, we must stagger the cell connection along the $2b$ side by a half length $b$ [see Fig. 7(c)]. A connected pair of triangles can now rotate together as a single square up to 45°, enabling the double cell to be mobile. A row can then be fashioned by repeating the staggered layout with as many cells as are required. A second row is formed by adding cells above or below the first row, which always results in e-cones from adjacent cells sharing a common boundary along their bases. During folding, these bases have to move away from each other and upward, so this boundary must be cut as a slit from the outset. This

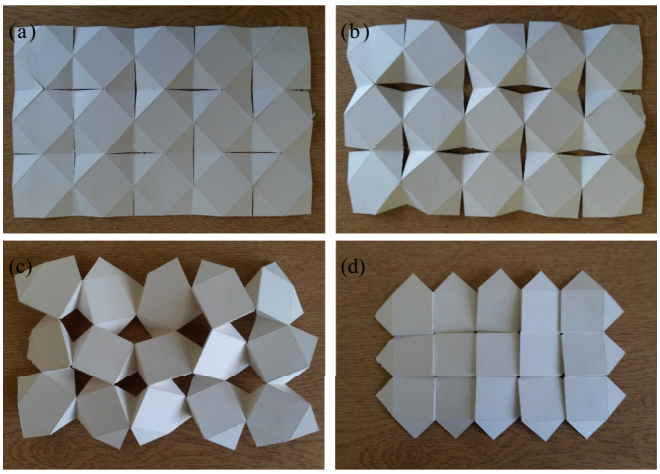


FIG. 8. Folding of a sheet made with the unit cell layout of Fig. 7(d). (a) Initial configuration where diagonal fold lines are mountain folds and the rest are valley folds: These have been reversed compared to Fig. 7 because we have turned the sheet over and the slits open into the page. (b) and (c) Progressive folding of the sheet until it becomes fully closed with (d) e-cones tucked flat underneath.

slit is formed at 90° to the usual central slit, giving two slit configurations in the final sheet. The first and second rows, and so forth, are nevertheless physically connected by adjacent triangles forming as interior squares in the usual way: Because the fold lines run to the corners of the original unit cell, they run continuously over the entire sheet, making overall folding and construction more efficient.

A paper card demonstrator made in this way is given in Fig. 8, which shows the initial planar configuration, intermediate folded shapes, and its closed state. The sheet has been turned over so that closed e-cones can be tucked underneath. What is not apparent from the figure is the natural cooperation in folding across the sheet once the fold lines have been fully formed by flexing a few times: It clearly behaves as a single degree-of-freedom system. This is keenly evinced when the sheet is turned over again so that e-cones fold upward; by pinching two or three e-cones shut, the rest of the sheet obligingly folds into its closed state. For this geometry, the in-plane contraction from the initial state is $1/\sqrt{2}$ in both directions, giving an effective Poisson ratio that is negative. The final state can be simply unfolded by extending in two directions.

## IV. CONCLUSION

We have thought about how shallow deformations of a slit thin sheet may be used to mobilize interesting kinematics in a folded sheet with a pattern of slits. Our approach has been mainly discursive because we wanted to highlight how we might synthesize interesting behavior informally. We have moved from continuous displacement fields (at least outside of the slit) to folded shapes, from unit cells to full sheets, and the results of a simple discrete elastic model of an e-cone are not too far from the actual shape properties of a continuum e-cone, by itself and when it is part of the deforming k-cone motif. The behavior of our material demonstrator is also elegant and definitive but there is much more to learn and try. Clearly, we can tinker with the layout of slits and fold line patterns to achieve different local deformations where, for example, not all e-cones may need to fold vertically. The negative Poisson ratio effect is an auxetic characteristic that can be tuned by varying this layout and there is the possibility of engendering a net variation of out-of-plane shape to give discrete approximations of doubly curved surfaces. Cutting, as well as folding, we believe, enhances the much lauded capability and potential of origami-inspired engineering structures, most notably by enabling net Gaussian curvature. There are also practical questions on endowing them with stiffness, if required, using realistic engineering materials; we may even wish to actuate the folding process by embedding motors or smart material elements such as shape memory alloys. These remain exciting avenues of further work for our sheets.

[1] J. W. Wang, Rim curvature anomaly in thin conical sheets revisited, Phys. Rev. E **84**, 066603 (2011).
[2] E. Cerda and L. Mahadevan, Conical surfaces and crescent singularities in crumpled sheets, Phys. Rev. Lett. **80**, 2358 (1998).
[3] E. Efrati, L. Pocivavsek, R. Meza, K. Y. C. Lee, and T. A. Witten, Confined disclinations: Exterior vs material constraints in developable thin elastic sheets, Phys. Rev. E **91**, 022404 (2015).
[4] M. Kleman and J. Friedel, Disclinations, dislocations and continuous defects: A reappraisal, Rev. Mod. Phys. **80**, 61 (2008).
[5] F. Lechenault and M. Adda-Bedia, Generic Bistability in Creased Conical Surfaces, Phys. Rev. Lett. **115**, 235501 (2015).
[6] J. Chopin and A. Kudrolli, Disclinations, e-cones, and their interactions in extensible sheets, Soft Matter **12**, 4457 (2016).
[7] M. Ben Amar and Y. Pomeau, Crumpled paper, Proc. R. Soc. London A **453**, 729 (1997).
[8] M. M. Muller, M. Ben Amar, and J. Guven, Conical Defects in Growing Sheets, Phys. Rev. Lett. **101**, 156104 (2008).
[9] E. Cerda, L. Mahadevan, and J. M. Pasini, The elements of draping, Proc. Natl. Acad. Sci. USA **101**, 1806 (2004).
[10] M. F. Ashby and D. R. H. Jones, *Engineering Materials 1: An Introduction to Their Properties and Materials*, 2nd ed. (Butterworth-Heinemann, Oxford, 1996).
[11] R. J. Lang, *The Complete Book of Origami* (Dover, New York, 1988).
[12] S. M. Farmer and C. R. Calladine, Geometry of "developable cones", Int. J. Mech. Sci. **47**, 509 (2005).
[13] K. A. Seffen, Fundamental conical defects: The d-cone, its e-cone and its p-cone, Phys. Rev. E **94**, 013002 (2016).
[14] C. R. Calladine, *Theory of Shell Structures* (Cambridge University Press, Cambridge, 1983).
[15] V. Brunck, F. Lechenault, A. Reid, and M. Adda-Bedia, Elastic theory of origami-based metamaterials, Phys. Rev. E **93**, 033005 (2016).

[16] A. Lamoureux, K. Lee, M. Shlian, S. R. Forrest, and M. Shtein, Dynamic kirigami structures for integrated solar tracking, Nat. Commun. **6**, 8092 (2015).

[17] D. M. Sussman, Y. Cho, T. Castle, X. Gong, E. Jung, S. Yang, and R. D. Kamien, Algorithmic lattice kirigami: A route to pluripotent materials, Proc. Natl. Acad. Sci. USA **112**, 7449 (2015).